Evaluation of an ^{111}In-Radiolabeled Peptide as a Targeting and Imaging Agent for ErbB-2 Receptor–Expressing Breast Carcinomas

Senthil R. Kumar,[1] Thomas P. Quinn,[1] and Susan L. Deutscher[1,2]

Abstract

Purpose: The cellular targeting and tumor imaging properties of a novel ErbB-2-avid peptide, discovered from bacteriophage display, were evaluated in human breast carcinoma cells and in breast carcinoma–xenografted mice.

Experimental Design: The affinity of the ErbB-2 targeting peptide KCCYSL and its alanine substituted counterparts for the extracellular domain (ECD) of purified recombinant ErbB-2 (ErbB-2-ECD) was assessed by fluorescence titration. Binding of the KCCYSL peptide to breast and prostate carcinoma cells was analyzed by confocal microscopy. A DOTA(GSG)-KCCYSL peptide conjugate was radiolabeled with ^{111}In, and stability, target binding, and internalization were analyzed *in vitro*. *In vivo* biodistribution and single-photon emission computed tomography imaging studies were done with the radiolabeled peptide in MDA-MB-435 human breast tumor–bearing severe combined immunodeficient mice.

Results: KCCYSL peptide exhibited high affinity (295 $\pm$ 56 nmol/L) to ErbB-2-ECD. Substitution of alanine for lysine, tryptophan, and cysteine reduced the peptide affinity $\sim$ 1- to 2.4-fold, whereas replacing leucine completely abolished binding. Both biotin-KCCYSL and ^{111}In-DOTA(GSG)-KCCYSL were capable of binding ErbB-2–expressing human breast carcinoma cells *in vitro*. Approximately 11% of the total bound radioactivity was internalized in the carcinoma cells. Competitive binding studies indicated that the radiolabeled peptide exhibited an IC_{50} value of 42.5 $\pm$ 2.76 nmol/L for the breast carcinoma cells. ^{111}In-DOTA(GSG)-KCCYSL was stable in serum and exhibited rapid tumor uptake (2.12 $\pm$ 0.32 %ID/g) at 15 min postinjection and extended retention coupled with rapid whole body disappearance, as observed by biodistribution and single-photon emission computed tomography imaging studies, respectively.

Conclusions: The DOTA(GSG)-KCCYSL peptide has the potential to be used as a tumor-imaging agent and a vehicle for specific delivery of radionuclide or cytotoxic agents for tumors overexpressing ErbB-2.

Breast cancer remains a major cause of cancer morbidity and mortality in women throughout the world (1). Patients at risk for cancer recurrence are individuals with nodal positive tumors and aggressive tumor phenotypes, defined as high or intermediate grade, endocrine receptor negative, and/or Her2/neu positive (2). Aberrant expression of the epidermal growth factor receptor (ErbB-1) or closely related ErbB-2 (Her2/neu) receptor has been implicated in the formation of various malignancies including breast cancer.

The ErbB-2 proto-oncogene encodes the 185-kDa protein receptor ErbB-2 (3). ErbB-2, along with three other known homologous proteins, ErbB-1, ErbB-3, and ErbB-4, form the ErbB family (or subclass I) of receptor tyrosine kinase (3). ErbB-2 is frequently overexpressed in epithelial cancers and its overexpression is associated with poor clinical outcome (4). The ligands for the growth factor receptor tyrosine kinase family are numerous yet similar (5). All of them are structurally homologous and contain an epidermal growth factor–like motif with six cysteines at highly conserved positions defining three disulfide loops that give rise to the tricyclic nature of these proteins (6). However, no natural ligand has been found that binds directly to ErbB-2. ErbB-2 is a shared coreceptor for several stromal ligands. Blocking the action of ErbB-2 may thus inhibit a myriad of mitogenic pathways affecting ErbB-expressing tumor cells (7). Although ErbB-2 is expressed at low levels in several normal organs and tissues (8), the elevated levels of ErbB-2 in many human malignancies and its extracellular accessibility make it an attractive target for the development of tumor-specific agents.

The ErbB-2 receptor has been targeted by a variety of substances and modalities, including monoclonal antibody (mAb; ref. 9), immunoconjugates (10), vaccines (11), and

Authors' Affiliations: [1]Department of Biochemistry, University of Missouri-Columbia and [2]Harry S. Truman Veterans Hospital, Columbia, Missouri

Received 1/22/07; revised 7/30/07; accepted 8/3/07.

Grant support: NIH P50 grant CA103130-01 and a Merit Review Award from the Veterans Administration (S.L. Deutscher).

The costs of publication of this article were defrayed in part by the payment of page charges. This article must therefore be hereby marked *advertisement* in accordance with 18 U.S.C. Section 1734 solely to indicate this fact.

Requests for reprints: Susan L. Deutscher, Department of Biochemistry, M743 Medical Sciences Building, University of Missouri-Columbia, Columbia, MO 65212. Phone: 573-882-2454; Fax: 573-884-4597; E-mail: deutschers@missouri.edu.

doi:10.1158/1078-0432.CCR-07-0160

antisense and gene therapy (12). Herceptin (trastuzumab; Genentech), a humanized mAb against ErbB-2 (13), was the first such agent to reach widespread clinical use, in particular for the treatment of metastatic breast cancer (13, 14). However, the drug has shown cardiotoxicity in some patients (15). Peptides, in contrast to large molecules such as antibodies, are known to exhibit less toxicity and possess better pharmacokinetic properties such as higher target-to-background ratios and faster blood clearance (16, 17). A number of regulatory peptide analogues that bind receptors, such as somatostatin (18) and α melanocortin-1 (19), on tumors are being actively pursued in imaging and therapy studies. Advances in powerful combinatorial technologies such as bacteriophage (phage) display have provided new approaches for identifying cancer-targeting biomolecules. Random peptide libraries displayed on phage can be effectively screened for sequences that bind a particular antigen or receptor. A number of peptides that bind receptor molecules, oncoproteins, integrins, and tumor-associated carbohydrates have been identified using phage display libraries (20–24). Phage display technology has also been used to optimize binding affinities of heregulin variants for the ErbB-3 receptor (25). In our previous study (26), we identified peptides from phage display libraries that bound the recombinant extracellular domain of human ErbB-2 (ErbB-2-ECD). One of the isolated peptides, the six-amino-acid KCCYSL sequence, represented 75% of the selected population and exhibited limited nonlinear homology with several proteins that potentially could interact with the ErbB family of receptors. Sequence analysis suggested that the KCCYSL peptide may also act as a mimetic of a CCY/F motif present in the epidermal growth factor–like domain of ErbB ligands (26). The peptide specifically recognized recombinant ErbB-2-ECD and human carcinoma cells overexpressing ErbB-2. Therefore, we hypothesized that the KCCYSL peptide has the potential to be used as an imaging agent as well as a vehicle for specific delivery of radionuclide or cytotoxic agents to ErbB-2–overexpressing tumors for diagnostic and therapeutic purposes.

In the present study, the specificity, affinity, and key binding residues of KCCYSL peptide were investigated. The optimized peptide sequence was radiolabeled with ^{111}In and analyzed for binding cultured MDA-MB-435 breast carcinoma cells. Furthermore, the biodistribution of the ^{111}In-DOTA(GSG)-KCCYSL peptide and its ability to act as a single-photon emission computed tomography (SPECT) imaging agent were explored *in vivo* in mice bearing human MDA-MB-435 breast tumors.

Materials and Methods

Materials. The anti-ErbB-2-ECD mAb (immunoglobulin G2b, clone 42) was purchased from BD Transduction Laboratories. α-Tubulin antibody (11H10) was procured from Cell Signaling Technology. Unless specifically noted, all other reagents were purchased from Sigma Chemical Co.

Expression and purification of recombinant ErbB-2-ECD. The expression and purification of the ErbB-2-ECD was done as previously described (26). The identity of the ErbB-2-ECD was confirmed by immunoblot analysis with anti-ErbB-2 mouse mAb. The purified protein was stored in PBS and NaN_3 (0.02%).

Peptide synthesis. All peptides were synthesized using the Advanced Chem Tech 396 multiple peptide synthesizer using solid-phase Fmoc chemistry. For radiolabeling studies, the bifunctional chelator DOTA (Macrocyclic, Inc.) was coupled to the NH_2 terminus of the linear KCCYSL or KYLCSC (scrambled) peptide with a Gly-Ser-Gly (GSG) amino acid spacer between DOTA and the NH_2-terminal lysine of the peptide. Peptides were purified by reverse-phase high-pressure liquid chromatography (RP-HPLC) on a C_{18} column (218TP54; Vydac), lyophilized, and stored at -20°C. Identities of the peptides were confirmed by electrospray ionization-mass spectrometry (Mass Consortium Group). Carboxyfluorescein succinimidyl ester (5-FAM)–conjugated (GSG)-KCCYSL and (GSG)-KYLCSC peptides were synthesized by AnaSpec.

Fluorescence assay. Fluorescence titration experiments were carried out using a Photon Technology International instrument (Deltascan Illumination system) interfaced to a Dell Computer equipped with Felix fluorescence analysis software. The titrations were done at 25°C with varying amounts of peptide added to a fixed ErbB-2-ECD concentration (0.5 μmol/L) in 2-mL PBS (pH 7.4). Each measurement was collected for 5 to 20 s after 1 to 2 min of pre-equilibration. The excitation shutter remained closed during pre-equilibration of the sample and was opened only during data acquisition to minimize photobleaching of the sample. Fluorescence measurements were corrected for dilutions and photobleaching of ErbB-2-ECD. Intrinsic tryptophan fluorescence of the ErbB-2-ECD was monitored at an excitation wavelength of 300 nm and an emission wavelength of 350 nm, respectively. Binding affinity was calculated using the Langmuir equation and GraphPad Prism 3.0 software and expressed as $K_d \pm$ SD.

Cell lines and cell culture. The MDA-MB-435 human breast carcinoma cell line, isolated from a pleural effusion (27), the prostate carcinoma cell line (PC3), and the K-562 human erythroid leukemia cell line were obtained from American Type Tissue Culture. The cells were maintained as monolayer cultures in RPMI 1640 supplemented with 10% fetal bovine serum, sodium pyruvate, nonessential amino acids, and L-glutamine. The cultures were maintained at 37°C in a 5% CO_2 humidified incubator. Subculturing was done using standard trypsinization procedures.

Cell-surface binding and immunodetection of proteins. Cell binding studies were done as previously described (26). Briefly, the slides containing cells were incubated with various concentrations of biotinylated KCCYSL peptide [0.1-1 μmol/L, 0.01 mol/L Tris (pH 7.5), 1% bovine serum albumin]. After three washes, 10 μg/mL neutravidin-Texas red (Molecular Probes) in 0.01 mol/L Tris (pH 7.5), 0.5% bovine serum albumin was added for 1 h at room temperature in the dark. Laser scanning confocal microscopy was done with an excitation/emission wavelength of 596/620 nm with a Bio-Rad MRC confocal microscope (Molecular Cytology Core Facility, University of Missouri).

The detection of ErbB-2 protein in different cell lysates was done by immunoblotting (26) with anti-ErbB-2-ECD mAb (immunoglobulin G2b, clone 42). The immunoreactive proteins were developed with peroxidase-conjugated antimouse ErbB-2 and antirabbit (α-tubulin) antibodies and visualized by chemiluminescence detection system (Pierce). The bands were quantitated (Quantity 1 software) with an imager system (Bio-Rad Molecular Imager ChemiDoc XRS system).

Radiolabeling of DOTA(GSG)-KCCYSL peptide. The ^{111}In labeling of DOTA(GSG)-KCCYSL or DOTA(GSG)-KYLCSC peptide was done as follows. Briefly, 5 μL of $^{111}InCl_3$ (185 MBq/500 μL in 50 mmol/L HCl; Mallinckrodt), 80 μL of ammonium acetate (0.1 mol/l; pH 5.5), and 25 μg of DOTA(GSG)-KCCYSL were mixed and incubated at 85°C for 60 min. After this, an aliquot of 2 mmol/L EDTA (10 μL) was added to the reaction mixture to complex unreacted ^{111}In. Radiolabeling efficiency ranged from 40% to 50%. The resulting conjugate was purified by RP-HPLC with a linear gradient of 10% to 95% acetonitrile/0.1% trifluoroacetyl or trifluoroacetic acid for 30 min. Purified preparations were flushed with nitrogen gas to remove the acetonitrile, and the pH was adjusted to neutral by adding 0.2 mol/L sodium phosphate (pH 8.0)/0.15 mol/L NaCl. To avoid oxidation of peptide cysteine thiols, tris(2-carboxyethyl)phosphine hydrochloride (0.1 mmol/L) was added to the peptide stock solution.

Peptide stability. The stability of the radiolabeled complex was evaluated in 0.01 mol/L PBS containing 0.1% bovine serum albumin (pH 7.4) at 37°C for various times (1, 2, 4, 6, and 12 h) and monitored for degradation by HPLC. The radiolabeled peptide conjugate stability was also tested in mouse serum by incubating 11.1 MBq of ^{111}In-DOTA(GSG)-KCCYSL in 500 μL of serum at 37°C for 30 min, 1 h, and 2 h, respectively. Subsequently, the samples were centrifuged at 12,500 rpm and 25-μL aliquots of the supernatant were analyzed by RP-HPLC.

In vitro ***cell binding of radiolabeled KCCYSL peptide.*** Cell binding of the radiolabeled peptide was evaluated by *in vitro* receptor binding assays with ErbB-2–expressing human breast carcinoma (MDA-MB-435) and ErbB-2–negative K-562-human erythroid leukemia cell lines. Cells grown in culture flasks were trypsinized and released. After washing once with cell binding medium [MEM with 25 mmol/L HEPES (pH 7.4), 0.2% bovine serum albumin, 3 mmol/L 1,10-phenathroline], cells (1×10^6 per tube) were transferred to small Eppendorf tubes and further incubated at 37°C for different time intervals (30 min, 1 h, 2 h, 4 h, and 6 h) with 5×10^4 cpm radiolabeled peptide in 0.3-mL binding medium. After incubation, the binding medium was aspirated and the cells were rinsed with ice-cold 0.01 mol/L PBS/0.2% bovine serum albumin (pH 7.4) and centrifuged. This process was repeated at least thrice to remove excess unbound radioactivity. The radioactivity bound to the cells was counted in a gamma counter (Wallac). The cell-binding capacity was reported as total radioactivity (cpm) that was bound to the cells. As a negative control, cell binding experiments were also done with a radiolabeled scrambled peptide variant, KYLCSC.

To determine the ligand concentrations that inhibit 50% of the maximum specific binding (IC_{50}), competition experiments were done with radiolabeled DOTA(GSG)-KCCYSL peptide and its nonradiolabeled congener. Cells (1×10^5 per tube) were incubated at 37°C with 6×10^4 cpm of ^{111}In-DOTA(GSG)-KCCYSL peptide and different concentrations (10^{-5}-10^{-12} mol/L) of the nonradioactive ^{111}In-DOTA(GSG)-KCCYSL peptide in 0.3 mL of binding medium. After incubation, the medium containing the cells was centrifuged and the supernatant was aspirated. The pellet was washed twice with 0.5 mL of ice-cold binding buffer and the radioactivity in the pellet was measured in a gamma counter. The IC_{50} values for the peptide were calculated by using Grafit software (Erithacus Software Ltd.).

Internalization experiments. Cellular internalization of the radiolabeled peptide was analyzed in MDA-MB-435 cells at 37°C, at which all metabolic processes including receptor internalization are active. Cells (3×10^5 per tube) were incubated with ^{111}In-DOTA(GSG)-KCCYSL (4×10^4 cpm) and, at different times (15 min, 30 min, 1 h, 1.5 h, and 2 h), the cells were centrifuged and the pellet was washed twice with ice-cold cell binding medium to remove any unbound activity. The pellet was further rinsed in 1.2% cold acetic acid (pH 2.5) containing saline, vortexed, and incubated for 5 min on ice. Cells were pelleted by centrifugation. The supernatant, which contains the surface-bound peptide, was then collected. Radioactivity in both the supernatant and cell pellet (internalized radioactive peptide) was measured in a gamma counter. The total surface-bound and internalized radioactivity (cpm) was depicted as a function of time. Fluorescent peptide binding and internalization in MDA-MB-435 cells was also analyzed with 5-FAM–labeled specific and scrambled peptides (0.5 μmol/L) at 37°C for 45 min. After washing, the cells were fixed in paraformaldehyde and analyzed by confocal microscopy with an excitation/emission wavelength of 490/520 nm.

Biodistribution studies. All animal studies were done in compliance with federal and local institutional rules for the conduct of animal experimentation. Severe combined immunodeficient (SCID) mice were implanted s.c. in the shoulder with MDA-MB-435 breast carcinoma cell (1×10^7) suspensions with >90% viability. Each mouse ($n = 3$) per time point was injected with ~ 0.11 MBq of the ^{111}In-DOTA(GSG)-KCCYSL peptide through the tail vein. After radioactivity administration, the mice were housed separately. Groups of three mice were sacrificed at different times (15 min, 1 h, 2 h, 4 h, and 24 h) after injection, and then tissues of interest were collected. The contents of the gastrointestinal tract were not removed. Whole-body and tissue samples were weighed and their radioactivity was measured in a gamma counter. The total blood volume was calculated as 6.5% of the whole body weight. Radioactivity uptake in the tumor and normal tissues of interest was expressed as a percentage of the injected radioactive dose per gram (%ID/g) or as %ID of tissue. For blocking experiments, the tumor mice were preinjected with 100 μg of DOTA(GSG)-KCCYSL peptide labeled with 1×10^{-4} mol/L nonradioactive ^{111}In. Fifteen minutes after injection of the nonradiolabeled peptide, 0.11 MBq of radiolabeled counterpart was injected and the blocking efficiency was evaluated after 2 h. Statistical comparisons between groups were done with unpaired Student's t test. $P \leq 0.005$ was considered statistically significant.

MicroSPECT/CT imaging studies. MDA-MB-435 tumor xenografts were established by injecting 1×10^7 cells in the shoulder region of SCID mice. Tumor-bearing mice were injected in the tail vein with 11.1 MBq of ^{111}In-DOTA(GSG)-KCCYSL or ^{111}In-DOTA(GSG)-KYLCSC peptide. The mice were sacrificed 2 h postinjection and imaged with a CTI Concord Microsystems microSPECT scanner (CTI Concorde Microsystems). Acquisition time was 2 h and the images were reconstructed using a filtered backprojection reconstruction algorithm. The SPECT images were fused with conventional microCT (IMTEK, Inc.) images to validate regions of increased radiolabeled ligand uptake.

Results

Binding affinity of KCCYSL peptide variants to ErbB-2-ECD. To identify the crucial amino acid residues in the hexameric peptide KCCYSL that are required for the structural interaction with ErbB-2-ECD, alanine substitutions were introduced at all positions in the KCCYSL peptide. Fluorescence quenching experiments were done with the alanine-substituted peptides to evaluate the equilibrium dissociation constant (K_d) that described the binding affinity. Intrinsic tryptophan fluorescence of the protein was monitored as a function of peptide concentration. To minimize the influence of tyrosine emission on tryptophan fluorescence, the samples were excited at 300 nm and monitored at 350 nm.

The fluorescence data indicated that the peptides bound to ErbB-2-ECD with varying affinities (Fig. 1). Change in the affinity of the peptide for ErbB-2-ECD was minimal when one or both of the cysteine residues were replaced with alanine. The affinities of KAAYSL, KACYSL, and KCAYSL were 305, 344, and 387 nmol/L, respectively, whereas the originally selected peptide exhibited an affinity of 295 nmol/L for ErbB-2-ECD. The fold decrease in the affinity with respect to the original KCCYSL peptide was moderate to high when alanine was substituted for tyrosine in the fourth position (1.8-fold) and lysine substituted in the first position (2.4-fold). The K_d obtained for the peptides KCCASL (Tyr-Ala) and ACCYSL (Lys-Ala) was 710 and 932 nmol/L, respectively. Further, substitution of leucine with alanine (KCCYSA) in the sixth position at the COOH terminus of the peptide resulted in complete loss of its ability to bind to ErbB-2-ECD.

Previous studies have suggested that incorporation of proline at both ends of a peptide could enhance function due to proper presentation and/or a reduction in the number of possible conformations of the peptide (28). In the present study, incorporation of two proline residues on either end of the KCCYSL peptide, however, did not improve the affinity (K_d = 760 nmol/L) toward ErbB-2-ECD. Therefore, the KCCYSL peptide originally identified via phage display selections was used in subsequent studies.

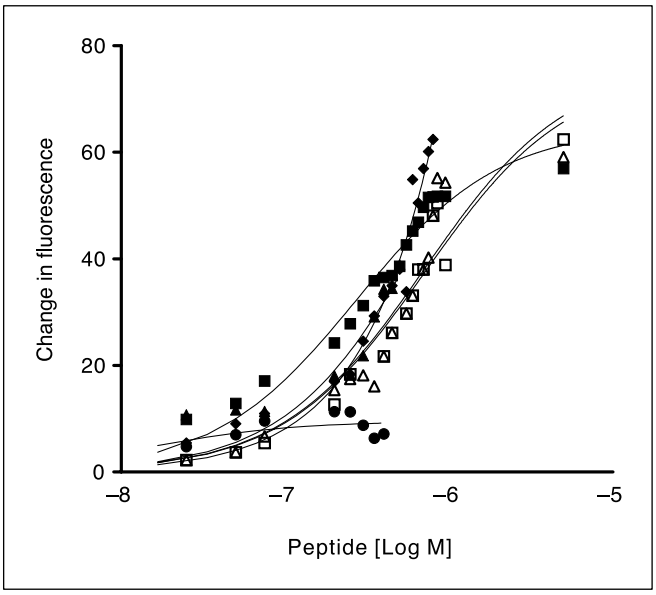

Fig. 1. Intrinsic fluorescence quenching of purified recombinant ErbB-2-ECD (0.5 μmol/L) was done in the presence of different peptides in a dose-dependent manner. □, KCCYSL, K_d = 295 ± 56 nmol/L; ♦, KCCYAL, K_d = 560 ± 19 nmol/L; ●, KCCYSA, K_d = no binding; ▲, PKCCYSLP, K_d = 714 ± 30 nmol/L; △, KCCASL, K_d = 932 ± 10 nmol/L; ○, ACCYSL, K_d = 714 ± 30 nmol/L. Affinity (K_d) was calculated by using the Langmuir binding equation and was reported as K_d ± SD. Error bars are eliminated for clarity. Points, mean of three replicates.

Cell binding studies. MDA-MB-435 human breast and PC3 human prostate carcinoma cell lines, both of which are known to express ErbB-2 protein, and the ErbB-2–negative K-562 leukemia cells were chosen for the cell binding assays (29). The ability of the biotinylated KCCYSL peptide to recognize these cells was analyzed by confocal microscopy. The erythroid leukemia cell line K-562, the ErbB-2–negative cell line (30), was used as a negative control cell line. The KCCYSL peptide at a concentration of 300 nmol/L bound both breast (MDA-MB-435) and prostate (PC3) carcinoma cells but did not bind ErbB-2–negative erythroid leukemia (K-562) cells, indicating the selectivity of the peptide for the ErbB-2 oncoprotein–expressing cells (Fig. 2A). Binding was observable at lower peptide concentrations (<100 nmol/L) but with relatively less intensity. The expression patterns of ErbB-2 in these cell lines were confirmed by immunoblottiing experiments shown in Fig. 2B. Experiments were also done to ascertain whether trastuzumab (Herceptin), an ErbB-2–specific antibody, could block the binding of biotin-KCCYSL to MDA-MB-435 cells by confocal microscopy. In equimolar concentrations of the antibody and the peptide (3×10^7 mol/L), no inhibition of the peptide binding to the cells was observed (data not shown), indicating that the peptide binding region and antibody epitope(s) on ErbB-2 are distinct.

Radiolabeling, stability, and* in vitro *binding of the KCCYSL peptide. The macrocyclic chelator DOTA was conjugated to the NH_2 terminus of the peptide so that the molecule could be radiolabeled independent of the peptide sequence. DOTA was selected because of its ability to chelate a wide variety of imaging and therapeutic radiometals. To avoid any steric hindrance by DOTA, a GSG spacer was introduced between DOTA and the NH_2 terminus of KCCYSL. Synthetic DOTA(GSG)-KCCYSL peptide was labeled with $^{111}InCl_3$ and purified to homogeneity by C_{18} RP-HPLC (Fig. 3A). Stability of the radiolabeled peptide in 0.01 mol/L PBS (pH 7.4) was examined. The radiolabeled DOTA(GSG)-KCCYSL peptide was radiochemically stable for 12 h in PBS, as determined by RP-HPLC analysis (data not shown). RP-HPLC analysis was also done to analyze the metabolic stability of the radiolabeled peptide incubated in mouse serum for different time intervals (Fig. 3B). The radiolabeled peptide peak eluted at the same time point as the native peptide at all time points tested. However, the ^{111}In-DOTA(GSG)-KCCYSL peptide peak was reduced by 50% at 2 h relative to the radioactivity peak at 0 h. There was also a small radiopeak eluting early at all time points tested. This peak is likely to be nonspecific radioactivity that coelutes with free ^{111}In in HPLC analysis.

In vitro cell binding experiments were done to confirm the binding ability of the radiolabeled peptide before *in vivo* pharmacokinetic studies. We chose to analyze the binding of radiolabeled peptide to MDA-MB-435 breast carcinoma cells because these cells overexpress ErbB-2, are highly tumorigenic in animals, and would serve as a human breast tumor model for imaging. The receptor-binding activity of the radiolabeled peptide to MDA-MB-435 human breast carcinoma cells as a function of time was done *in vitro* by incubating radiolabeled peptide conjugate (6×10^4 cpm) with MDA-MB-435 cells (1×10^6 per well) for various times at 37°C. Binding of the peptide to the cells increased gradually, reaching a saturation by 2 h. No significant increase in binding was observed after this time, indicating saturable binding of the peptide to the cells. Cell binding capacity of 28% to 30% was obtained for the peptide with respect to the initial total radioactivity added to the MDA-MB-435 carcinoma cells (Fig. 4A). Similar studies with K-562 cells (ErbB-2 negative) did not show appreciable binding, indicating that the radiolabeled peptide was specific for ErbB-2–expressing human breast cancer cells ($P < 0.001$). A radiolabeled scrambled peptide KYLCSC did not bind either cell line (Fig. 4A).

Specificity of binding of the radiolabeled peptide to MDA-MB-435 carcinoma cells was determined by competition experiments in the presence of various concentrations of nonradioactive In-DOTA(GSG)-KCCYSL peptide. Binding of the peptide to the breast cancer cells decreased in a concentration-dependent manner in the presence of the non-radiolabeled congener, as indicated by a decrease in bound radioactivity (Fig. 4B). Evaluation of the binding data indicated that radiolabeled ^{111}In-DOTA(GSG)-KCCYSL exhibited an IC_{50} value for MDA-MBA-435 breast carcinoma cells of 42.5 ± 2.76 nmol/L.

It can be argued that a radioactive drug would function optimally if the diagnostic/therapeutic dose could be residualized within the cell on tumor binding (31). The ability of MDA-MB-435 carcinoma cells to internalize the bound radiolabeled ^{111}In-DOTA(GSG)-KCCYSL by receptor-mediated endocytosis was analyzed. Results indicated that there was a progressive accumulation of total radioactivity inside cells (Fig. 4C). The cell-surface associated radioactivity increased until 2 h. After removal of surface-bound radioactivity, ~11% of the total bound radioactivity remained internalized. Most peptide binding occurred on the cell surface ($P < 0.001$).

In addition, studies with fluorescently labeled KCCYSL also indicated that the majority of peptide biding occurred on the cell surface and showed minimal internalization in MDA-MB-435

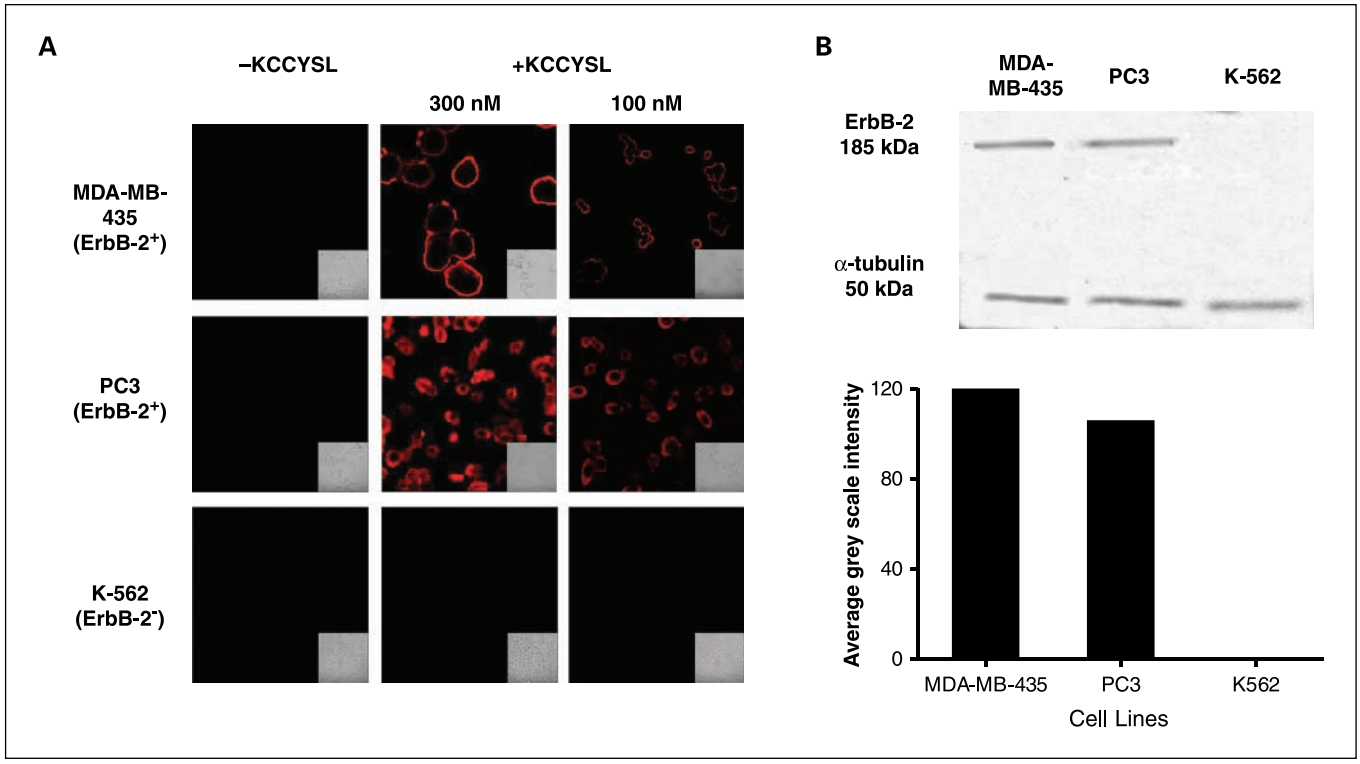

Fig. 2. Binding of biotinylated linear hexameric KCCYSL peptide to cancer cells with and without ErbB-2 receptor surface expression. *A,* laser confocal scanning microscopic examination of cell -surface binding of linear KCCYSL peptide (300 and 100 nmol/L) was done. Controls without peptide did not show any fluorescence with all cell lines. Addition of peptide revealed binding to breast (MDA-MB-435) and prostate (PC3) carcinoma cells (ErbB-2 positive) but not to K-562 human chronic myeloid leukemia cells (ErbB-2 negative). *B,* ErbB-2 expression in different cell lines. Forty micrograms of protein from MDA-MB-435, PC3, and K-562 cell lysates were used to determine the level of ErbB-2 protein expression. After visualizing ErbB-2 protein by enhanced chemiluminescence, the membrane was stripped and reprobed for α-tubulin protein. Densitometric analysis was done with Bio-Rad Quantity 1 software.

breast carcinoma cells (Fig. 4D). The fluorescently labeled scrambled peptide did not bind or was not internalized in MDA-MB-435 cells.

In vivo *biodistribution studies.* Biodistribution of the ^{111}In-DOTA(GSG)-KCCYSL peptide was examined in MDA-MB-435 breast tumor–bearing athymic SCID mice. The tumor and organ distribution properties of the radiolabeled peptide at 15 min, 1 h, 2 h, 4 h, and 24 h after injection are depicted in Table 1. Tumor uptake of the radiolabeled peptide was 2.12 ± 0.32, 0.78 ± 0.09, and 0.66 ± 0.11 %ID/g at 30 min, 1 h, and 2 h, showing tumor retention of the radiolabeled ligand. Radioactivity levels in the blood were 3.61 ± 0.33 %ID/g at 15 min postinjection, followed by a rapid clearance by the end of 2 h (0.13 ± 0.03 %ID/g). Rapid tumor uptake and blood clearance kinetics resulted in a tumor-to-blood ratio of 5.0 at the end of 2 h, a value that is 7.4 times higher than the ratio (0.67) obtained 15 min postinjection. Whole-body disappearance of radioactivity was equally rapid, with 66% ID in the urine 15 min postinjection and 93% ID after 1 h. Normal organ uptake of radioactivity was highest in the kidneys because they were the primary route of excretion. Radioactivity in the kidneys declined from a peak of 10.51 ± 0.07 %ID/g at 15 min postinjection to 5.26 ± 0.78 at 1 h, remaining steady between 5.75 ± 0.69 and 6.45 ± 0.69 for the next 3 h. Excluding the kidneys, only the lungs displayed any appreciable retention of radioactivity. Lung radioactivity was 3.18 ± 0.16 %ID/g at 15 min postinjection, decreasing to 0.23 ± 0.17 %ID/g at 4 h,

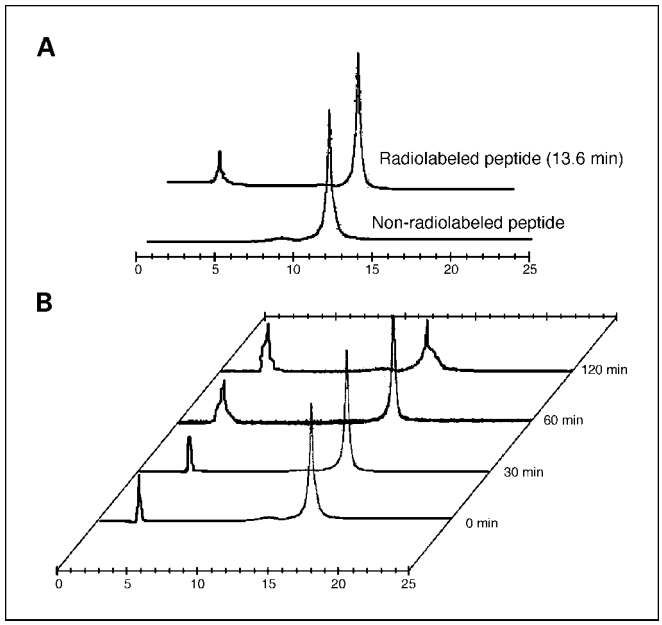

Fig. 3. RP-HPLC elution profile of ^{111}In-DOTA(GSG)-KCCYSL peptide. *A,* the nonradiolabeled peptide eluted at 12.5 min whereas the radiolabeled conjugate eluted later at 13.6 min. *B,* serum stability of the radiolabeled peptide. Purified ^{111}In-DOTA(GSG)-KCCYSL peptide was incubated at 37°C for different times in mouse serum. An aliquot from the incubation mixture was analyzed by RP-HPLC to examine the integrity of the peptide. The radiolabeled peak seemed to be intact at least up to 60 min.

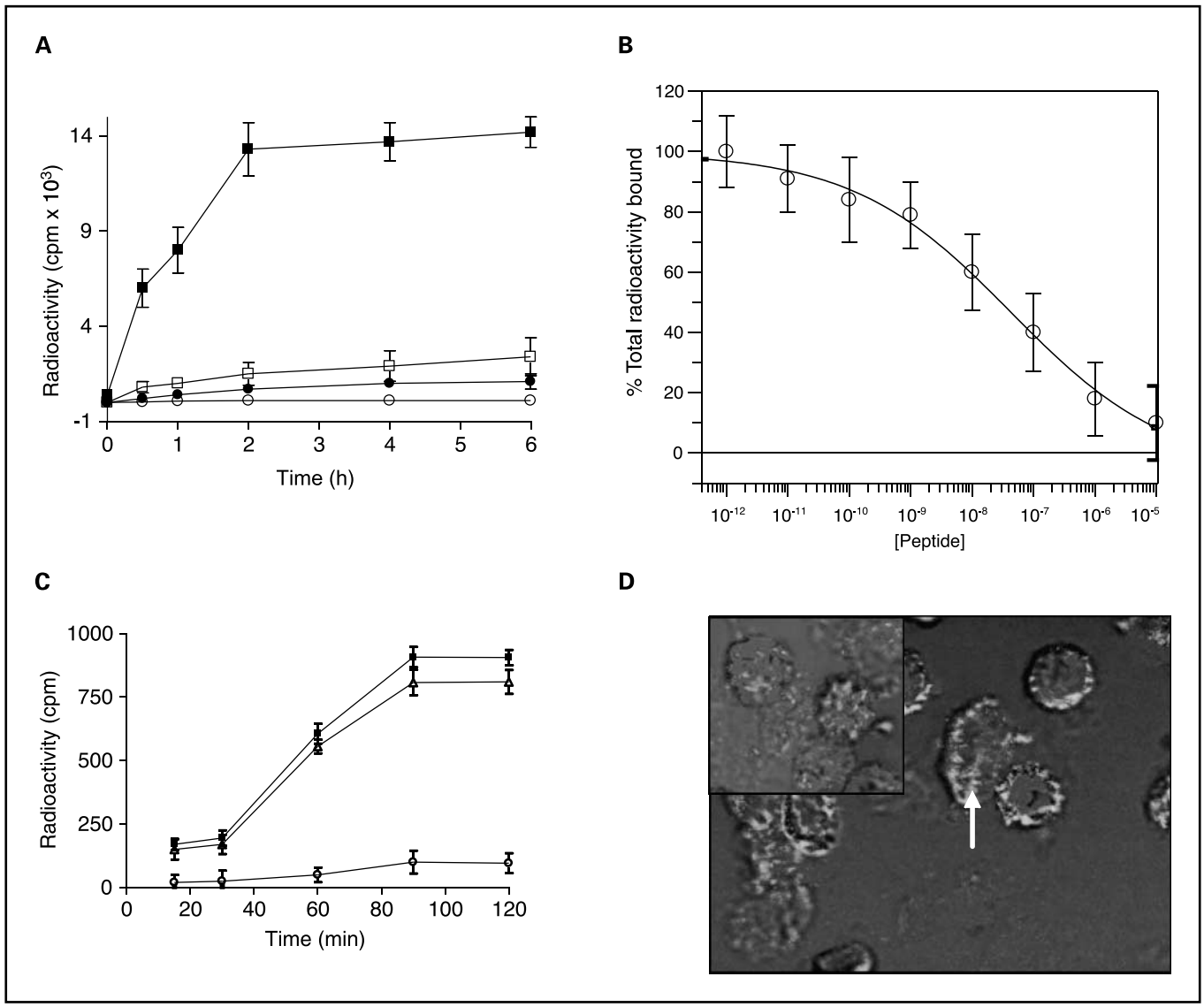

Fig. 4. The ErbB-2 receptor binding properties of the radiolabeled ^{111}In-DOTA(GSG)-KCCYSL. *A,* ~1.0 × 10^6 cells per well were incubated at 37°C for different time intervals with 5 × 10^4 cpm radioligand. Whereas significant radioligand binding to human MDA-MB-435 breast carcinoma cells was observed (■), minimal binding was observed with K-562 human chronic myeloid leukemia cells (●). Little binding of a radiolabeled scrambled peptide KYLCSC was observed with MDA-MB-435 (□) or K-562 (○) cell lines. Points, mean of three replicates; bars, SD. $P < 0.001$. *B,* displacement of ^{111}In-DOTA(GSG)-KCCYSL peptide by its nonradiolabeled counterpart. MDA-MB-435 cells were incubated with 6 × 10^4 cpm radioligand and increasing concentrations of the nonradioactive peptide. The IC_{50} value obtained was 42.5 ± 2.76 nmol/L. Points, mean of three replicas; bars, SD. *C,* determination of percent internalized radioactivity in human MDA-MB-435 breast carcinoma cells. Cells (3 × 10^5 per tube) were incubated at 37°C with ^{111}In-DOTA-(GSG) KCCYSL (4 × 10^4 cpm). The total (■), surface-bound (△), and internalized (○) radioactivity (cpm) as a function of time is depicted. Points, mean of two replicates; bars, SD. $P < 0.001$. *D,* surface binding and internalization of 5-FAM(GSG)-KCCYSL peptide. MDA-MB-435 cells were incubated with 0.5 μmol/L fluorescent peptide for 45 min at 37°C. After washing, the cells were fixed in paraformaldehyde and analyzed by confocal microscopy with an excitation/emission wavelength of 490/520 nm. The majority of the peptide was surface bound. Arrow, potential internalized peptide. Inset, analysis with FAM(GSG)-KYLCSC peptide indicated no binding.

which was below the 4-h tumor value (0.33 ± 0.05 %ID/g). There was very little radioactive retention in the remaining vital organs, muscle, or bone. An examination of the tumor-to-blood and tumor-to-muscle ratios indicated that there was a significant increase during the first 2 h postinjection.

SPECT/CT tumor imaging. The tumor targeting abilities of ^{111}In-DOTA(GSG)-KCCYSL and ^{111}In-DOTA(GSG)-KYLCSC were evaluated in SCID mice bearing ErbB-2–positive MDA-MB-435 breast tumors. A whole-body SPECT/CT scan was done at 2 h postinjection (Fig. 5A-C). The breast tumor was clearly visualized, as were the kidneys with ^{111}In-DOTA(GSG)-KCCYSL, which was coincident with the pharmacokinetics of the radiolabeled peptide (Table 1). On the other hand, the radiolabeled ^{111}In-DOTA(GSG)-KYLCSC scrambled peptide did not image the tumor (Fig. 5A), showing the sequence specificity of the KCCYSL peptide. Magnetic resonance imaging studies suggested that ^{111}In-DOTA (GSG)-KCCYSL can image small tumors (~70.0 mm^3). Additional experiments are under way to determine the lower limits of detection.

The specificity of tumor uptake of the radiolabeled peptide *in vivo* was further evaluated by carrying out competition experiments with its unlabeled congener. MDA-MB-435 tumor mice (n = 3) were injected via the tail vein with nonradioactive In-DOTA(GSG)-KCCYSL, followed 15 min later by its radioactive

^{111}In-peptide homologue. Simultaneously, another set of mice (n = 3) were injected with only the radiolabeled peptide, which served as a positive control. The results shown in Fig. 5D indicated that the tumor uptake of radiolabeled peptide was blocked by 50% in mice injected with the nonradioactive peptide (P = 0.0012). The presence of excess nonradioactive peptide did not affect the percentage of radioactivity uptake per gram of tissue in the normal organs including the lungs and kidneys (data not shown). No significant amount of radioactivity was observed in the remaining organs, highlighting the rapid whole-body disappearance of the administered radioactive peptide. These results showed that the tumor uptake specific for KCCYSL peptide was receptor mediated, and the radioactivity in the kidneys and lungs was non–peptide specific.

Discussion

We characterized the *in vitro* and *in vivo* binding properties of the peptide KCCYSL. The peptide was previously selected from phage display libraries against the ECD of the tumor-associated ErbB-2 antigen. The KCCYSL peptide bound human recombinant ErbB-2-ECD with nanomolar affinity and also bound both human breast and prostate carcinoma cells that overexpress the ErbB-2 antigen. More importantly, an ^{111}In-radiolabeled version of the linear peptide localized and successfully imaged MDA-MB-435 xenografted tumors in SCID mice. Alanine scanning studies indicated that substitution of the tyrosine or cysteine residues in the KCCYSL sequence moderately affected the peptide affinity for ErbB-2, suggesting that these residues may help to either maintain peptide integrity or target recognition. These results are in keeping with previous studies that suggested that the two cysteines and a semiconservative aromatic amino acid (Y/F) are invariant in all of the ErbB family ligands (26). Substitution of leucine with alanine completely abolished binding to ErbB-2-ECD, indicating that hydrophobic interactions may be a major force in ligand recognition. The originally selected KCCYSL peptide bound better to both purified ErbB-2 and ErbB-2–expressing cell lines than any of the alanine-substituted peptides examined in this study.

A DOTA-conjugated peptide was synthesized for radiolabeling with the γ-emitting radionuclide ^{111}In for *in vivo* preclinical SPECT imaging of breast tumors. The ^{111}In-DOTA(GSG)-KCCYSL peptide contained a GSG linker at the NH_2-terminal end of the peptide. DOTA strongly chelates a variety of β or γ particle–emitting radiometals, including ^{111}In, which is often used in SPECT imaging studies (32). Radiolabeling of the DOTA-conjugated peptide was rapid and yielded a highly radiochemical pure compound. Both buffer and serum stability studies were done and revealed good chemical stability at least up to 1 h. The metabolic degradation of the radiolabeled peptide observed at 2 h could be attributed to plasma peptidases. The observed instability of the radiolabeled peptide(s) in serum after 1 h is not uncommon or surprising because the chemically synthesized linear peptide contains only natural amino acids, which are susceptible to proteolysis (31). Peptides on filamentous phage are presented as fusion proteins to stable coat proteins and are therefore protected against proteolysis (33). The ^{111}In-DOTA(GSG)-KCCYSL peptide bound well to the ErbB-2–positive MDA-MB-435 breast carcinoma cells whereas binding to nonreceptor expressing cells was negligible. Binding was sequence specific in that a radiolabeled scrambled peptide variant (KYLCSC) did not bind the carcinoma cells.

Competition studies with unlabeled peptide showed the specificity of the radiolabeled peptide for the breast carcinoma cells. A portion (11%) of ^{111}In-DOTA(GSG)-KCCYSL was internalized in MDA-MB-435 cells. This suggests that the majority of peptide binding occurs on the cell surface, as the rapid turnover of the receptor population available on the cell surface guarantees that there are always surface receptors capable of interacting with the ligand present in the extracellular space (34). Moreover, recent mathematical modeling of

Table 1. Pharmacokinetics of ^{111}In-DOTA(GSG)-KCCYSL in MDA-MB-435 breast tumor–bearing SCID mice

Tissues	15 min	1 h	2 h	4 h	24 h
Percentage injected dose/gram (%ID/g)					
Tumor	2.12 ± 0.32	0.78 ± 0.09	0.66 ± 0.11	0.33 ± 0.05	0.10 ± 0.02
Brain	0.15 ± 0.04	0.03 ± 0.01	0.02 ± 0.01	0.04 ± 0.05	0.00 ± 0.00
Blood	3.61 ± 0.33	0.40 ± 0.09	0.13 ± 0.03	0.11 ± 0.09	0.01 ± 0.00
Heart	1.34 ± 0.14	0.22 ± 0.04	0.10 ± 0.05	0.04 ± 0.01	0.04 ± 0.01
Lung	3.18 ± 0.17	0.82 ± 0.14	0.57 ± 0.18	0.23 ± 0.19	0.14 ± 0.03
Liver	0.92 ± 0.05	0.25 ± 0.06	0.22 ± 0.02	0.19 ± 0.03	0.13 ± 0.01
Spleen	0.56 ± 0.26	0.14 ± 0.03	0.12 ± 0.06	0.05 ± 0.03	0.07 ± 0.00
Kidneys	10.51 ± 0.07	5.26 ± 0.78	5.75 ± 0.69	6.45 ± 0.69	3.43 ± 0.62
Muscle	0.51 ± 0.25	0.09 ± 0.02	0.03 ± 0.02	0.09 ± 0.10	0.02 ± 0.00
Pancreas	0.96 ± 0.07	0.10 ± 0.02	0.06 ± 0.03	0.05 ± 0.02	0.03 ± 0.00
Bone	0.97 ± 0.02	0.20 ± 0.03	0.09 ± 0.06	0.07 ± 0.03	0.05 ± 0.01
Percentage injected dose (%ID)					
Stomach	0.39 ± 0.09	0.15 ± 0.12	0.10 ± 0.05	0.09 ± 0.02	0.03 ± 0.01
Intestines	0.74 ± 0.07	0.30 ± 0.16	0.29 ± 0.05	0.29 ± 0.03	0.09 ± 0.01
Urine	66.5 ± 1.40	93.78 ± 0.85	93.74 ± 1.94	96.25 ± 0.80	97.9 ± 0.10
Uptake ratio of tumor/normal tissue					
Tumor/blood	0.58	1.95	5.10	3.00	10.0
Tumor/muscle	4.10	8.70	22.00	3.70	0.5

NOTE: The data are presented as percentage injected dose/gram or as percentage injected dose (mean ± SD, n = 3).

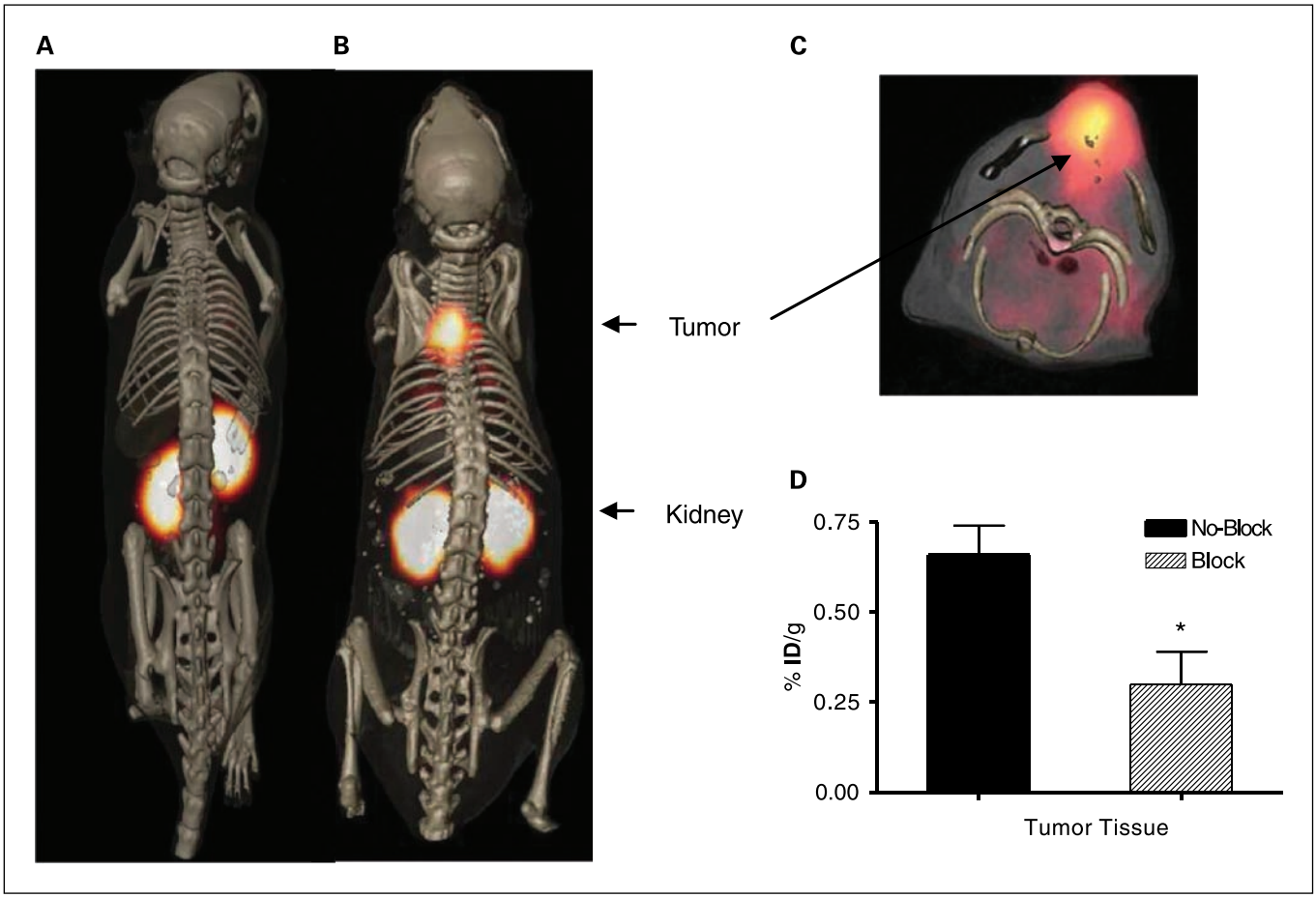

Fig. 5. Tumor imaging with ^{111}In-DOTA(GSG)-KCCYSL peptide. MDA-MB-435 breast tumor – xenografted SCID mice were injected in the tail vein with 11.1 MBq of ^{111}In-DOTA(GSG)-KCCYSL or ^{111}In-DOTA(GSG)-KYLCSC scrambled peptide and imaged in a microSPECT scanner. The SPECT images were fused with conventional microCT images to validate regions of increased radiolabeled ligand uptake. *A,* coregistered microSPECT/CT radioligand uptake image with ^{111}In-DOTA(GSG)-KYLCSC; *B,* coregistered microSPECT/CT image with ^{111}In-DOTA(GSG)-KCCYSL; *C,* microSPECT/CT image axial view focusing on tumor uptake of the radioligand. *D, in vivo* blocking studies with ^{111}In-DOTA(GSG)-KCCYSL in MDA-MB-435 breast tumor – xenografted SCID mice. Fifteen minutes after injection of the nonradiolabeled In-DOTA(GSG)-KCCYSL (10^{-5}-10^{-12} mol/L) peptide, 0.11 MBq of radiolabeled counterpart was injected and the blocking efficiency was evaluated after 2 h. A 50% block of the radiolabeled peptide binding to the tumor tissue was observed. Columns, mean of three animals for each experiment; bars, SD. *, $P < 0.001$.

ErbB-2 trafficking has been interpreted in favor of decreased internalization and increased recycling of ErbB-2 (35). It has also been reported that in the human breast cancer cell line SKBR3, the ErbB-2 receptors are internalization resistant and stably associated with membrane protrusions (36).

On the other hand, the ability of cells to internalize the radioligand is favorable for radiopharmaceutical application of peptides and for imaging studies and may contribute to prolonged retention in tumor tissue (34). Herceptin, a humanized mAb against ErbB-2, which is widely used in treatment of breast cancer, is believed to exert its antitumor effect by internalizing ErbB-2 receptors and preventing recycling (37). Our studies with KCCYSL peptide suggest that only very minimal internalization occurred in the cells. This internalization may mimic the action of Herceptin on binding ErbB-2. However, peptide binding to MDA-MB-435 breast carcinoma cells was not blocked by equivalent concentrations of Herceptin (data not shown). It is not clear whether the entire receptor population is readily accessible for the peptide ligand on the cell surface, which may be critical for the process of effective internalization. Further studies are required to confirm the mechanism of action of the peptide on the ErbB-2 receptor internalization or recycling process.

In vivo characterization of the radiolabeled peptide included biodistribution studies as well as SPECT/CT imaging. Biodistribution studies indicated that the clearance of unbound radioactivity was rapid and occurred exclusively via the urinary tract. Such rapid clearance is a contributing factor to the high target-to-nontarget tissue ratios observed in the MDA-MB-435 xenografts. Furthermore, the stability of the chelating moiety also contributed to low background radioactivity levels; otherwise, free ^{111}In would be retained on metal-binding proteins present in the serum and would show slow clearance from the circulation. There seemed to be virtually no clearance through the hepatobiliary system. Nonspecific retention of radioactivity in other organs was very low, although the lungs did exhibit some retention. Radioactivity in the lungs was non–peptide specific and may be due to the contribution of the blood pool because the lungs were highly perfused. There was a high level of accumulation of the radioconjugate in the kidneys, perhaps due to peptide breakdown via lysosomal degradation within

renal cells (38). Earlier studies with a ^{111}In-diethylenetriaminepentaacetic acid-cholecystokinin-B receptor targeting peptide suggested that kidney homogenates are capable of metabolizing the peptide conjugate rapidly and thoroughly *ex vivo* (34). Alternately, the positively charged lysine in the peptide could contribute to nonspecific radioactivity retention in the kidneys (19). Moreover, high renal radioactive uptake could be caused by free sulfhydryls or a disulfide bond moiety (39). Coinjection of lysine or an amino acid cocktail could be pursued in future studies for decreasing unnecessary kidney uptake. This procedure has been shown to reduce nonspecific kidney retention associated with radiolabeled peptides and antibody fragments (40, 41).

In vivo SPECT/CT imaging studies with ^{111}In-DOTA(GSG)-KCCYSL revealed excellent tumor-homing propensity in mice xenografted with MDA-MB-435 human breast carcinoma cells. The majority of the radioactivity was detected in the tumor or in the kidneys. Very low whole-body, hepatobiliary, or pulmonary radioactivity was observed, highlighting the potential of this peptide for *in vivo* tumor imaging. In fact, this ErbB-2 tumor–targeting peptide is one of the first phage display–selected peptides other than the vasculature-targeting peptides (42) that have been used successfully in tumor imaging *in vivo*. In 2000, a report concluded that peptides isolated from phage display do not bind with high retention to tumors *in vivo* (43). Since then, a few studies have reported sequences from phage libraries that target neuroblastomas and prostate tumors *in vivo*; however, in these cases, the target antigens remain unknown (44, 45). The successful imaging of ErbB-2–expressing human breast carcinomas in SCID mice is a major step forward in developing cancer cell–associated imaging agents from phage display–selected peptides.

In conclusion, the findings reported here indicate that ^{111}In-DOTA(GSG)-KCCYSL shows promise for clinical use in tumor-targeted drug delivery and as a class of tracer for clinically imaging tumors on the basis of tumor-associated ErbB-2 expression.

Acknowledgments

We thank Tiffani Shelton, Dr. Said Figueroa, and Dr. Lixin Ma for their assistance with animal studies and imaging; Marie Dickerson for technical assistance; and the VA Biomolecular Imaging Center at the Harry S. Truman Veterans Affairs Medical Center and the University of Missouri-Columbia for their support.

References

1. Tsongalis GJ, Ricci A, Jr. Breast cancer as a model of realistic challenges in pharmacogenomics. Clin Biochem 2003;36:89–94.
2. Ross JS, Fletcher JA. The HER-2/neu oncogene in breast cancer: prognostic factor, predictive factor, and target for therapy. The Oncologist 1998;3:237–52.
3. McInnes C, Sykes BD. Growth factor receptors: structure, mechanism, and drug discovery. Biopolymers 1997;43:339–66.
4. Ross JS, Fletcher JA. The Her-2/neu oncogene. prognostic factor, predictive factor and target for therapy. Semin Cancer Biol 1999;9:125–38.
5. Jones JT, Akita RW, Sliwkowski MX. Binding specificities and affinities of EGF domains for ErbB receptors. FEBS Lett 1999;447:227–31.
6. Taupin D, Wu DC, Jeon WK, et al. The trefoil gene family are coordinately expressed immediate-early genes: EGF receptor- and MAP kinase-dependent interregulation. J Clin Invest 1999;103:R31–8.
7. Olayioye MA, Neve RM, Lane HA, Hynes NE. The ErbB signaling network: receptor heterodimerization in development and cancer. EMBO J 2000;19:3159–67.
8. De Potter CR, Van Daele S, Van de Vijver MJ, et al. The expression of the neu oncogene product in breast lesions and in normal fetal and adult human tissues. Histopathology 1989;15:351–62.
9. Weiner LM, Clark JI, Davey M, et al. Phase I trial of 2B1, a bispecific monoclonal antibody targeting c-erbB-2 and FcγRIII. Cancer Res 1995;55:4586–93.
10. Jinno H, Ueda M, Enomoto K, et al. Effectiveness of an Adriamycin immunoconjugate that recognizes the C-erbB-2 product on breast cancer cell lines. Surg Today 1996;26:501–7.
11. Disis ML, Grabstein KH, Sleath PR, Cheever MA. Generation of immunity to the HER-2/neu oncogenic protein in patients with breast and ovarian cancer using a peptide-based vaccine. Clin Cancer Res 1999;5:1289–97.
12. Harris JD, Gutierrez AA, Hurst HC, Sikora K, Lemoine NR. Gene therapy for cancer using tumour-specific prodrug activation. Gene Ther 1994;1:170–5.
13. Baselga J, Norton L, Albanell J, Kim YM, Mendelsohn J. Recombinant humanized anti-HER2 antibody (Herceptin) enhances the antitumor activity of paclitaxel and doxorubicin against HER2/neu overexpressing human breast cancer xenografts. Cancer Res 1998;58:2825–31.
14. Cobleigh MA, Vogel CL, Tripathy D, et al. Multinational study of the efficacy and safety of humanized anti-HER2 monoclonal antibody in women who have HER2-overexpressing metastatic breast cancer that has progressed after chemotherapy for metastatic disease. J Clin Oncol 1999;17:2639–48.
15. Seidman A, Hudis C, Pierri MK, et al. Cardiac dysfunction in the trastuzumab clinical trials experience. J Clin Oncol 2002;20:1215–21.
16. Fischman AJ, Babich JW, Strauss HW. A ticket to ride: peptide Radiopharmaceuticals. J Nucl Med 1993;34:2253–63.
17. Landon LA, Zou J, Deutscher SL. Is phage display technology on target for developing peptide-based cancer drugs? Curr Drug Discov Technol 2004;1:113–32.
18. Bakker WH, Krenning EP, Reubi JC, et al. *In vivo* application of [^{111}In-DTPA-D-Phe-1]-octreotide for detection of somatostatin receptor-positive tumors in rats. Life Sci 1991;49:1593–601.
19. Miao Y, Owen NK, Whitener D, et al. *In vivo* evaluation of ^{188}Re-labeled α-melanocyte stimulating hormone peptide analogs for melanoma therapy. Int J Cancer 2002;101:480–7.
20. Doorbar J, Winter G. Isolation of a peptide antagonist to the thrombin receptor using phage display. J Mol Biol 1994;244:361–9.
21. Renschler MF, Wada HG, Fok KS, Levy R. B-lymphoma cells are activated by peptide ligands of the antigen binding receptor or by anti-idiotypic antibody to induce extracellular acidification. Cancer Res 1995;55:5642–7.
22. Murayama O, Nishida H, Sekiguchi K. Novel peptide ligands for integrin α6β1 selected from a phage display library. J Biochem Tokyo 1996;120:445–51.
23. Peletskaya EN, Glinsky G, Deutscher SL, Quinn TP. Identification of peptide sequences that bind the Thomsen-Friedenreich cancer-associated glycoantigen from bacteriophage display libraries. Mol Diversity 1996;2:13–8.
24. Peletskaya EN, Glinsky VV, Glinsky GV, Deutscher SL, Quinn TP. Characterization of peptides that bind the tumor-associated Thomsen-Friedenreich antigen selected from bacteriophage display libraries. J Mol Biol 1997;270:374–84.
25. Ballinger MD, Jones JT, Lofgren JA, et al. Selection of heregulin variants having higher affinity for the ErbB3 receptor by monovalent phage display. J Biol Chem 1998;273:11675–84.
26. Karasseva NG, Glinsky VV, Chen NX, Komatireddy R, Quinn TP. Identification and characterization of peptides that bind human ErbB-2 selected from a bacteriophage display library. J Protein Chem 2002;21:287–96.
27. Schmidt CM, Settle SL, Keene JL, et al. Characterization of spontaneous metastasis in an aggressive breast carcinoma model using flow cytometry. Clin Exp Metastasis 1999;17:537–44.
28. Kini RM, Evans HJ. A novel approach to the design of potent bioactive peptides by incorporation of proline brackets: antiplatelet effects of Arg-Gly-Asp peptides. FEBS Lett 1995;375:15–7.
29. Hynes NE, Stern DF. The biology of erbB-2/HER-2 and its role in cancer. Biochim Biophysica Acta 1994;1998:165–84.
30. Penuel E, Akita RW, Sliwkowski MX. Identification of a region within the ErB2/HER2 intracellular domain that is necessary for ligand-independent association. J Biol Chem 2002;277:28468–73.
31. Jain RK. Delivery of molecular and cellular medicine to solid tumors. J Control Release 1998;53:49–67.
32. Kwekkeboom DJ, Kooij PP, Bakker WH, Macke HR, Krenning EP. Comparison of ^{111}In-DOTA-Tyr3-octreotide and ^{111}In-DTPA-octreotide in the same patients: biodistribution, kinetics, organ and tumor uptake. J Nucl Med 1999;40:762–7.
33. Askoxylakis V, Zitzmann S, Mier W, et al. Preclinical evaluation of the breast cancer cell-binding peptide p160. Clin Cancer Res 2005;11:6705–12.
34. Aloj L, Caraco C, Panico M, et al. *In vitro* and *in vivo* evaluation of ^{111}In-DTPAGlu-G-CCK8 for cholecystokinin-B receptor imaging. J Nucl Med 2004;45:485–94.
35. Hendriks BS, Opresko LK, Wiley HS, Lauffenburger DA. Quantitative analysis of HER2-mediated effect on HER2 and EGFR endocytosis: distribution of homo and heterodimers depends on relative HER2 levels. J Biol Chem 2003;278:23343–51.
36. Hommelgaard AM, Lerdrup M, van Deurs B. Association with membrane makes ErbB2 an internalization-resistant receptor. Mol Biol Cell 2004;15:1557–67.

37. Rubin I, Yarden Y. The basic biology of HER2. Ann Oncol 2001;12:S3–8.
38. Tsai SW, Li L, Williams LE, at al. Metabolism and renal clearance of ^{111}In-labeled DOTA-conjugated antibody fragments. Bioconjugate Chem 2001;12:264–70.
39. Chen J, Cheng Z, Owen NK, et al. Evaluation of an ^{111}In-DOTA-rhenium cyclized a-MSH analog: a novel cyclic-peptide analog with improved tumor-targeting properties. J Nucl Med 2001;42:1847–55.
40. Behr TM, Goldenberg DM, Becker WS. Reducing the renal uptake of radiolabeled antibody fragments and peptides for diagnosis and therapy: present status, future prospects and limitations. Eur J Nucl Med 1998;25:201–12.
41. Behr TM, Sharkey RM, Juweid ME, et al. Reduction of the renal uptake of radiolabeled monoclonal antibody fragments by cationic amino acids and their derivatives. Cancer Res 1995;55:3825–34.
42. Arap W, Pasqualini R, Ruoslahti E. Cancer treatment by targeted drug delivery to tumor vasculature in a mouse model. Science 1998;279:377–80.
43. Kennel SJ, Mirzadeh S, Hurst GB, et al. Labeling and distribution of linear peptides identified using *in vivo* phage display selection for tumors. Nucl Med Biol 2000;27:815–25.
44. Zhang J, Spring H, Schwab M. Neuroblastoma tumor cell-binding peptides through random peptide phage display. Cancer Lett 2001;171:153–64.
45. Newton JR, Kelly KA, Mahmood U, Weisselder R, Deutscher SL. *In vivo* selection of phage for the optical imaging PC-3 human prostate carcinoma in mice. Neoplasia 2006;8:772–80.